

Interorbital charge transfers and Fermi-surface deformations in strongly correlated metals: models, BaVS_3 and Na_xCoO_2

Frank LECHERMANN^{1,2}, Silke BIERMANN¹, and Antoine GEORGES¹

¹*CPHT École Polytechnique, 91128 Palaiseau Cedex, France*

²*LPT-ENS, 24 Rue Lhomond, 75231 Paris Cedex 05, France*

Fermi-surface deformations in strongly correlated metals, in comparison to results from band-structure calculations, are investigated. We show that correlation-induced interband charge transfers in multi-orbital systems may give rise to substantial modifications of the actual Fermi surface. Depending in particular on the relative strength of the crystal-field splitting and of the Hund's exchange coupling, correlations may either reinforce orbital polarization or tend to compensate differences in orbital occupancies, as demonstrated by investigating a 2-band Hubbard model in the framework of dynamical mean field theory (DMFT). The physical implications of such interorbital charge transfers are then explored in two case studies: BaVS_3 and Na_xCoO_2 . By means of the DMFT in combination with the local density approximation (LDA) to density functional theory (DFT), new insights in the underlying mechanism of the metal-to-insulator transition (MIT) of BaVS_3 are obtained. A strong charge redistribution in comparison to LDA calculations, i.e., a depletion of the broader A_{1g} band in favor of the narrower E_g bands just above the MIT is found. In addition, the intriguing problem of determining the Fermi surface in the strongly correlated cobaltate system Na_xCoO_2 is discussed.

§1. Introduction

In recent times, theoretical investigations of systems with strong electronic correlations have become feasible in realistic settings by using the material-specific band structure input as a single-particle reference system.¹⁾ This also raises new questions, in particular concerning effects stemming from the multi-orbital character of realistic materials. As most physical properties of a specific material in the metallic state are determined by the electronic states close to the Fermi level, one of the key questions is how these states are affected by strong Coulomb correlations. It is a well-documented fact, e.g., in cuprates, that the competition of localization and itinerancy can result in the appearance of distinct areas on the Fermi surface with strikingly different physical properties of the low-energy excitations. In this work, we concentrate on a more basic aspect, namely how correlations may lead to a modification of the shape of the Fermi surface itself, due to interorbital charge transfers. These modifications may result in a major change of the low-energy physics, e.g., by inducing new instabilities.

The track record of density functional theory (DFT) in local (spin) density or generalized gradient approximation, L(S)DA or GGA^{*)}, promoted the effective single-particle approach to a standard tool for electronic structure investigations. Despite the many successes, this approach is generally inadequate for strongly cor-

^{*)} If not explicitly noted, it is understood in the following that in the present context the term 'LDA' covers all these different approximations to the exchange-correlation energy in DFT.

related systems, and qualitative as well as quantitative discrepancies are well documented. However, surprisingly, for many correlated metals, such as Sr_2RuO_4 ,²⁾ optimally doped cuprates, and several heavy-fermion systems,³⁾ the Fermi surface predicted by LDA is apparently in rather good agreement with experimental data. Of course, there are also famous counter examples, such as for instance the LDA-predicted hole pockets in fcc-Ni which are absent in experiment.^{4),5)} Nevertheless, the overall encouraging results for the Fermi surface obtained by LDA calculations provided 'empirical' confidence that the Fermi surface is little affected by strong correlations in many materials. In this paper, we want to draw attention to the fact that there are indeed cases where electronic correlations do have a significant influence on the relative orbital occupancies, and on the Fermi-surface shape. This may result in a dramatic change of the low-energy physics, e.g., by allowing for new nesting possibilities.

Consider first the simple case of a perfectly cubic material involving a degenerate t_{2g} multiplet. The effective single-particle (Kohn-Sham) hamiltonian can be diagonalized to yield the bands $\varepsilon_{\mathbf{k}}^m$ with orbital index m . Assuming a local (i.e. \mathbf{k} -independent) self-energy matrix, cubic symmetry implies: $\Sigma_{mm'}(\omega)=\delta_{mm'}\Sigma(\omega)$. Hence, the Fermi surface of the interacting system corresponds to the k -points such that: $\varepsilon_{\mathbf{k}}^m=\mu-\Sigma(0)$ (with μ the chemical potential), implying that all Fermi-surface sheets are shifted in the same manner by correlations. However, Luttinger's theorem⁶⁾ implies that the total volume of the Fermi surface is unchanged by interactions, and coincides with the *total* number of electrons. As a result, in this simplest case, each Fermi surface sheet cannot be changed by correlations and the relation $\mu-\Sigma(0)=\mu_0(n)$ must be satisfied (with μ_0 the chemical potential of the reference system corresponding to the given total electron number). This teaches us that, for perfect cubic symmetry and a degenerate multiplet, the Fermi surface can only be changed by correlations if the self-energy has strong \mathbf{k} -dependence. In contrast, when orbital degeneracies are lifted due to strong anisotropies or crystal-field effects, even a local self-energy matrix can in principle induce Fermi-surface deformations due to its multi-orbital (non-scalar) structure. The interacting Fermi surface is now determined by: $\det[\mu\delta_{mm'}-H_{\mathbf{k}}^{mm'}-\Sigma_{mm'}(0)]=0$. Even if the off-diagonal components of the self-energy are negligible, each Fermi-surface sheet can be affected in a different manner according to: $\varepsilon_{\mathbf{k}}^m=\mu-\Sigma_{mm}(0)$. Note that Luttinger's theorem does not apply to each sheet separately, i.e., the *partial* orbital occupancies n_m do not necessarily correspond to the respective volume of the different sheets (even for a diagonal Σ). However, physical intuition suggests that large correlation-induced interorbital charge transfers (i.e., changes of the partial n_m for a fixed $n=\sum_m n_m$), will be associated with strong Fermi-surface deformations, as confirmed by the studies below.

In this paper, we first explore the relevant processes and mechanisms that determine interband charge transfers in multi-orbital systems. Such charge transfers have been recently discussed by several authors.^{2),7),8),9),10),11)} With the vanadium sulfide compound BaVS_3 and the puzzling sodium cobaltates, we then discuss two examples of systems where such repopulations may drive Fermi-surface deformations that play an essential role for the relevant physical properties.

§2. Multi-orbital effects in correlated systems

In real materials, the particularities of the band structure can have substantial influence on the effect of correlations. Crystal-field splittings and anisotropies giving rise to partial densities of states with different bandwidths and shapes lead in general to different renormalizations of the different bands by the Coulomb interactions. The net results are charge transfers between different subbands induced by the Coulomb interactions and a modified Fermi surface as compared to an effective single-particle reference system, e.g., as given by the LDA. The shape of the Fermi surface and the different subband fillings are in general determined by the interplay of crystal-field splitting, bandwidth ratios (or more generally the shapes of the partial densities of states), hybridizations, Coulomb interactions – in particular Hund’s rule coupling – as well as the global filling of the system. On general grounds, the electrons tend to either avoid the high cost of Coulomb interactions or to compensate it by enlarging the kinetic energy. Since the Coulomb interactions are smaller for electrons in different orbitals, uniform occupations of the subbands are naturally favored by the multi-orbital interaction vertex. The difference between the intraorbital Coulomb interaction U and the interorbital one U' is mathematically related to the Hund’s rule integral J that describes the lowering of the Coulomb interaction by exchange between electrons with equal spins. ^{*)} Thus, a strong Hund’s rule coupling will generally lead to rather uniform partial occupations of the different subbands. The crystal-field splitting Δ , on the other hand, tends to orbitally polarize the system. As shown by Manini *et al.*¹³⁾ in the framework of a two-band Hubbard model, the relevant energy scale that has to be compared to the crystal-field splitting is the *renormalized* bandwidth, not the bare one. In a system close to the Mott transition, small crystal-field splittings can therefore be sufficient to induce a strong orbital polarization. Recently, this effect was shown⁷⁾ to be crucial to understand the insulating oxides LaTiO_3 and YTiO_3 .

The overall orbital charge distribution is thus the result of a competition between Hund’s coupling which tends to level out differences in the orbital occupations and crystal-field splittings which favor orbital polarization. This interplay is influenced by the band structure of the material: in narrow band systems or for large Coulomb interactions U the crystal-field splittings are likely to dominate and the system may eventually be driven into an orbitally polarized state. Moreover, in strongly anisotropic systems involving bands with very different bandwidths, correlation-induced band narrowing can be different in the various bands, also affecting the magnitude of the charge transfer. The final state is thus a subtle balance between the Hund’s rule coupling, the effective crystal-field splitting and the effective bandwidths of the subbands, the latter two renormalized by the Coulomb interactions.

To substantiate these qualitative expectations, we have studied the interplay of the crystal-field splitting and Hund’s rule coupling as a function of U in an anisotropic

^{*)} In t_{2g} systems, e.g., it can be shown that $U - U' = 2J$.¹²⁾

Hubbard model with two non-hybridizing bands:

$$\begin{aligned} \mathcal{H} = & \sum_{\langle i,j \rangle m\sigma} \left(t_{ij}^{(m)} - \mu\delta_{ij} \right) \hat{c}_{im\sigma}^\dagger \hat{c}_{jm\sigma} + \Delta \sum_{i\sigma} (\hat{n}_{i2\sigma} - \hat{n}_{i1\sigma}) \\ & + U \sum_{im} \hat{n}_{im\uparrow} \hat{n}_{im\downarrow} + U' \sum_{i\sigma} \hat{n}_{i1\sigma} \hat{n}_{i2\bar{\sigma}} + U'' \sum_{i\sigma} \hat{n}_{i1\sigma} \hat{n}_{i2\sigma} \quad , \end{aligned} \quad (2.1)$$

where $\hat{c}_{im\sigma}^\dagger$ ($\hat{c}_{jm\sigma}$) creates (annihilates) an electron with spin σ ($=\uparrow, \downarrow$) and orbital index m ($=1, 2$) at the i th site. The interorbital interactions U', U'' are described by combinations of the on-site Coulomb interaction U and the local Hund's coupling integral J . We chose the parametrization $U'=U-2J$ and $U''=U-3J$, proven to be suitable for t_{2g} substates.¹²⁾ Crystal-field effects are taken into account via the energy splitting 2Δ between the orbitals. Spin-Flip and pair-hopping terms were neglected in (2.1). For the numerical applications we choose the lattice to be the infinite-connectivity Bethe lattice giving rise to a semi-elliptical density of states (DOS) of bandwidth W_m for band m .

This model is treated within dynamical mean field theory (DMFT): the lattice model is mapped onto a local-impurity problem in an effective self-consistent bath. The self-consistency condition relates the local lattice Green's function to the impurity problem in the usual manner.¹⁴⁾ The impurity problem is solved using the quantum Monte-Carlo (QMC) Hirsch-Fye algorithm¹⁵⁾ with up to 128 slices in imaginary time τ and 10^6 sweeps.

In the following, n denotes the total filling, and n_1, n_2 the respective subband filling. Figure 1 shows results for the two-band model with different bandwidths (ratio $b=W_2/W_1=1/2$) in the absence of crystal-field splitting. The overall filling of one electron ($n=1$) is kept constant during the calculation, but the partial fillings change from their non-interacting values of $n_1 \sim 2/3$ and $n_2 \sim 1/3$. Figure 1a visualizes the non-interacting densities of states (DOS), while Fig. 1b displays the partial occupations of the two bands as a function of the Coulomb interaction U for different values of U/J . The overall tendency to equalization of the orbital occupancies with increasing Coulomb interaction and in particular close to the insulating regime at large U is a consequence of the bandwidths differences being less important the stronger the renormalizations become. We note that the quasiparticle residues Z_m , as extracted from the linear regime of the imaginary part of the self-energies on the Matsubara axis, are of similar magnitude (even if, interestingly the broad band is slightly stronger correlated, due to its bigger occupation). The influence of J which reinforces the orbital compensation is evident: for decreasing U/J ratios the orbital compensation effect is substantially more pronounced.

For small J – the effect is striking at $J=0$ but also present for selected U/J – a small- U regime is observed where increasing mutual electronic interactions first lead to further orbital polarization. This should stem from the fact that by increasingly populating the broader band the electrons can gain kinetic energy and thus may compensate the increased potential energy. To quantify this subtle balance more rigorously we have considered the above model in a static approximation which allows for an exact solution. We replace the operators by their mean values $\hat{n}_m \rightarrow \langle \hat{n}_m \rangle = n_m$

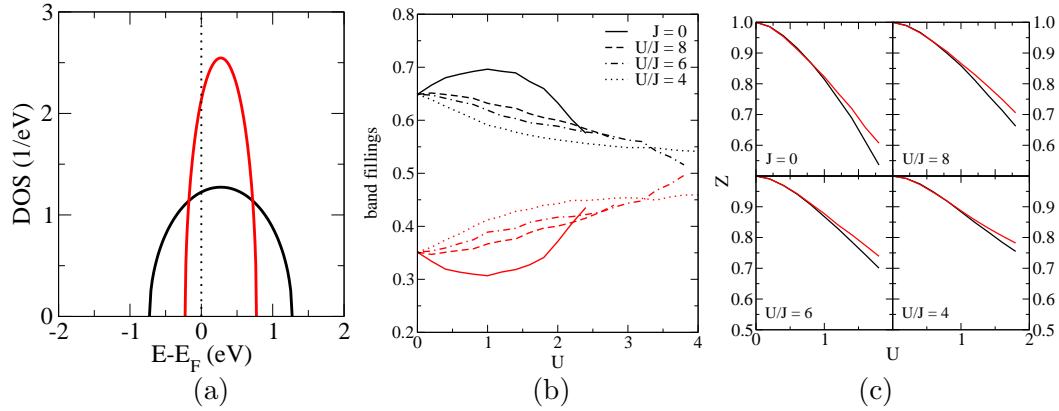


Fig. 1. Two-band model calculations with $W_2=0.5W_1$, $n=1$ and $\Delta=0$. (a) Non-interacting DOS. (b) Band fillings for different U/J series in the metallic regime. (c) Band-resolved QP residue for different U/J series. Dark (red) lines belong to properties of band 1(2).

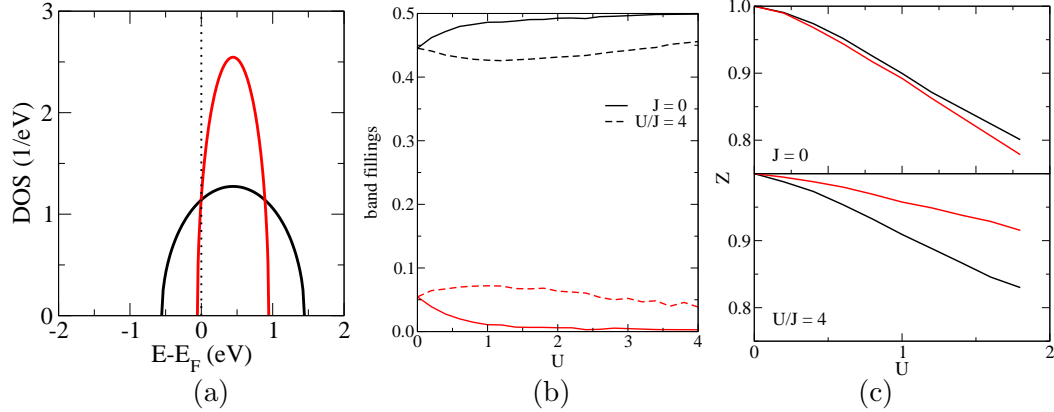


Fig. 2. Two-band model calculations in the incommensurate case with $W_2=0.5W_1$, $n=0.5$ and $\Delta=0$. (a) Non-interacting DOS. (b) Band fillings for $J=0$ and $U/J=4$ series in the metallic regime. (c) Band-resolved QP residue Z for both series. Dark (red) lines belong to properties of band 1(2).

and use a simple Friedel representation for the kinetic energy: $E_{\text{kin}} \sim n(2-n)$. From a minimization of the sum of the kinetic and on-site potential energy one obtains the occupations

$$n_1 = \frac{(1+b(n-1))W_1 - nU(1 - \frac{5}{a}) + 2\Delta}{(1+b)W_1 - 2U(1 - \frac{5}{a})}, \quad n_2 = n - n_1 \quad (2.2)$$

with $n=n_1+n_2$ and $a=U/J$. Choosing $b \leq 1$ and referring to $n_{1,0}$ as the occupation in the non-interacting case, the condition for $n_1 > n_{1,0}$ reads:

1. $a > 5$ for $\Delta > \frac{W_1}{4}(n-2)(1-b)$,
2. $a < 5$ for $\Delta < \frac{W_1}{4}(n-2)(1-b)$.

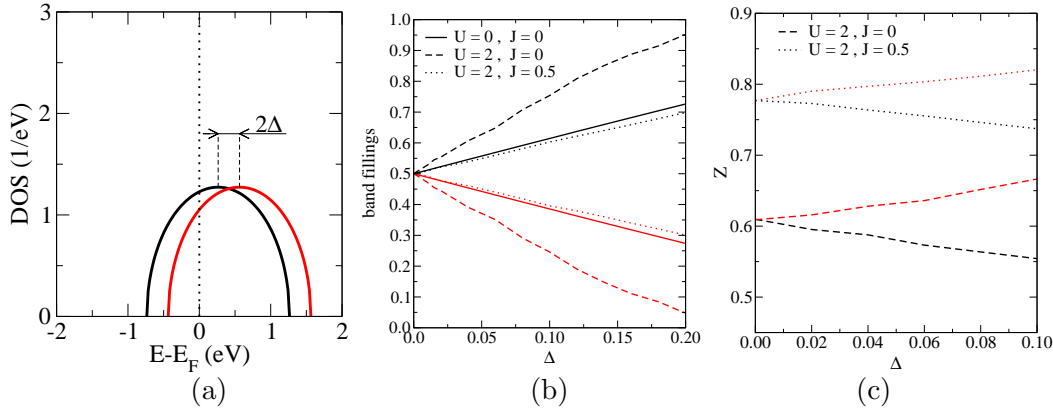


Fig. 3. Two-band model calculations with $W_2=W_1$, $n=1$ and varying crystal field Δ . (a) Non-interacting DOS. (b) Band fillings for different U , J settings in the metallic regime. (c) Band-resolved QP residue Z .

Independent of bandwidth, filling and crystal-field splitting, the system will thus polarize for $U/J > 5$ and compensate for $U/J < 5$, with respect to the non-interacting case. This limiting value can already be obtained while neglecting the kinetic-energy terms. It follows, e.g., from a Hartree-Fock treatment of the interaction term alone.^{8),10),11)} In fact, it can be shown that in the static limit the polarization/compensation regimes are in most cases independent of the specific form of the band energy. In the small- U regime where fluctuations are weak and the bandwidth renormalizations small, the static limit indeed describes the charge flow correctly (see Fig.1). However, for larger U dynamical effects and the changes in kinetic energy due to the bandwidth renormalizations become important: in this regime, the system tends to level out orbital occupation differences and eq. (2·2) no longer applies.

The situation is different for non-integer total filling n , (see Fig. 2). Though for small U the behavior is again qualitatively correctly described by (2·2), the system always tends to polarize in the large- U limit. Indeed, in the doped case there is no Mott transition and fluctuations are weaker, even for large U (Fig. 2c). Interestingly, there appears to be also a change in the degree of correlation for the different bands when turning on J .

Finally, we present results from calculations for a two-band model with finite crystal-field splitting and equal bandwidths $W_1=W_2$ in the commensurate case with $n=1$. Increasing Coulomb interactions drastically increase the orbital polarization, the stronger the larger the crystal field Δ . However, a large Hund's coupling J works against this polarization, as seen for $U/J=4$, which brings the orbital occupations back to their non-interacting values. As seen in Fig. 3c, the large differences in the occupations also give rise to substantially different quasiparticle residues Z_m .

From these model calculations we conclude that in general Coulomb interactions in non-degenerate multiband systems can induce substantial charge transfers between single subbands. Hund's rule coupling generally leads to a compensation of orbital occupation differences, whereas crystal-field splittings tend to polarize the system. The net charge flow depends on the fine balance of these effects, renormal-

ized by the Coulomb interactions and influenced by the anisotropies of the system. This explains, why indeed in some systems such as the series of $3d^1$ perovskite compounds studied in Ref. 7) correlations were found to orbitally polarize the system whereas in others (e.g. Sr_2RuO_4 ^{2),8)}) compensation effects were observed. Below we discuss two further recent examples, in which the question of orbital polarization or compensation effects acquires deeper importance by the fact, that the charge transfers induce substantial Fermi surface modifications: the first one is the vanadium sulfide compound BaVS_3 where the charge compensation effect was recently proposed⁹⁾ to be at the origin of a Fermi-surface modification that could be crucial for explaining the low-temperature properties of this compound. The second example is the thermoelectric cobaltate system Na_xCoO_2 , where very recent angle-resolved photoemission (ARPES) experimental data^{16),17)} seem to hint towards a charge polarization effect, whereas there are conflicting results concerning this issue from theoretical investigations of this problem.^{18),10),11)}

§3. The metal-insulator transition of BaVS_3

3.1. Brief overview of the physical properties of BaVS_3

BaVS_3 is well known as a long-standing challenging compound, exhibiting unusual electrical and magnetic properties.^{19),20),21),22),23),24)} At room temperature, this vanadium sulfide crystallizes in a hexagonal ($P6_3/mmc$) structure,²⁵⁾ whereby straight chains of face sharing VS_6 octahedra are directed along the c axis. Remarkably, BaVS_3 undergoes three distinct continuous phase transition with decreasing temperature. At $T_S \sim 240$ K the crystal structure transforms into an orthorhombic ($Cmc2_1$) structure (see Fig. 4),²⁶⁾ thereby creating an anisotropy in the ab -plane, i.e., perpendicular to the chain direction, and a zigzag distortion of the VS_3 chains in the bc -plane. Additionally, the sign of the Hall coefficient changes from negative to positive.²³⁾ The orthorhombic as well as the hexagonal unit cell both contain two formula units of BaVS_3 , whereby the relevant V atoms are equivalent by symmetry. The system displays a MIT at $T_{\text{MIT}} \sim 70$ K into a paramagnetic phase, hence BaVS_3 is an example where a MIT occurs without intervening magnetic ordering. Apparently, a magnetic transition finally takes place at $T_X \sim 30$ K, where an incommensurate antiferromagnetic order seems to be established.²⁷⁾

The paramagnetic conducting phase behaves as metallic ($d\rho/dT > 0$) above ~ 150 K, from where the resistivity²²⁾ (see Fig. 5) and the Hall coefficient²³⁾ (see Fig. 6) increase up to the MIT. From diffuse scattering experiments,²⁸⁾ correlated structural fluctuations along the direction of the VS_3 chains were deduced. These fluctuations were interpreted as a precursor for a commensurate charge density wave (CDW) instability associated with a possible Peierls mechanism that triggers the MIT. The obtained wave vector for the structural instability in the orthorhombic cell $\mathbf{q}_{\text{MIT}} = (1, 0, \frac{1}{2})_O$ is identical with the one derived by Inami *et al.*²⁹⁾ which indeed detected a doubling of the unit cell below T_{MIT} . In a recent x-ray study Fagot *et al.*³⁰⁾ were able to characterize the crystal structure below 70 K. The unit cell with a monoclinic distortion (space group Cm) now contains four formula units, whereby there

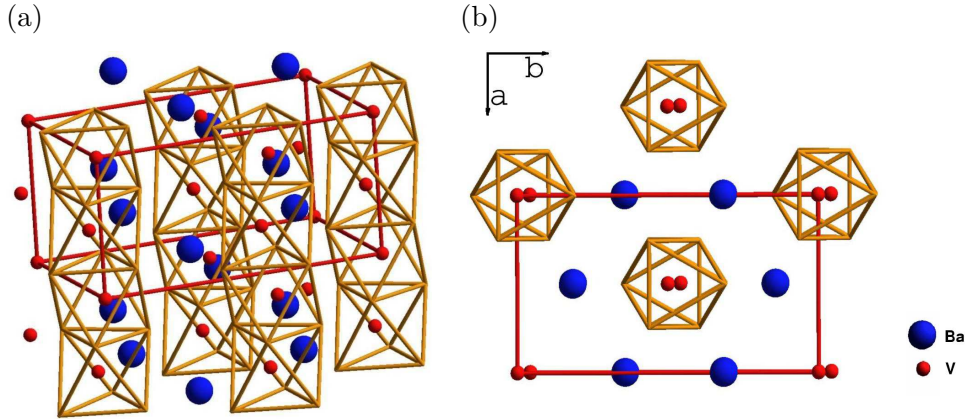


Fig. 4. BaVS_3 in the orthorhombic ($Cmc2_1$) structure. (a) 3D view, (b) view along the c axis.

appears to be a trimerization of the V atoms along the c axis, corresponding to a dominant $2k_F$ distortion.³¹⁾ It should be kept in mind however that the conduction anisotropy within the system is not strongly pronounced ($\sigma_c/\sigma_a \sim 3-4$),³²⁾ making pure 1D interpretations questionable. Furthermore, the “bad metal” regime above the MIT with the resistivity minimum at ~ 150 K is still not quite understood. In ultraviolet photoelectron-spectroscopic³³⁾ and photoemission^{34),35)} studies no Fermi edge was observed in the temperature regime around T_{MIT} . This raised some speculation about a possible realization of a Luttinger electron liquid in this compound, which however seems unrealistic due to the intriguing interplay of 3D and 1D features. The large increase of the Hall constant²³⁾ within the precursive regime seems to suggest that carriers are scattered into immobile states. In addition, an important feature of the phase above T_{MIT} is the existence of local moments as revealed by the Curie-Weiss form of the magnetic susceptibility.²²⁾ The effective moment corresponds approximately to one localized spin-1/2 per two V sites. Since the formal valence is V^{4+} , corresponding to one electron in the $3d$ -shell, this can be interpreted as the effective localization of half of the electrons. At T_{MIT} , the susceptibility rapidly drops, and the electronic entropy is strongly suppressed.³⁶⁾

The electronic structure close to the Fermi level in the orthorhombic ($Cmc2_1$) phase is dominated by low-lying $V(3d)-t_{2g}$ states. Due to symmetry, these states are split into one A_{1g} and two E_g states per V atom. First-principles DFT-LDA calculations for $Cmc2_1$ - BaVS_3 ³⁷⁾ do yield a $V(3d)$ - $S(3p)$ hybridization which is strong enough to account for the weak anisotropy of the transport properties. No band-gap opening has been reached within LDA. Instead, very narrow E_g bands right at the Fermi level, and a nearly filled dispersive band with mainly A_{1g} character extending along the c^* direction (\mathbf{c}^* is the reciprocal unit cell vector along the c axis of the system) have been found. This is consistent with a simple model proposed early on by Massenet *et al.*²⁰⁾ However, the occupancy of the narrow E_g bands found within LDA is too low to account for the observed local moment in the metallic phase. The nature of the CDW instability is also left unexplained by the LDA calculations. Indeed, the calculated norm of the Fermi wave vector of the broad A_{1g} band

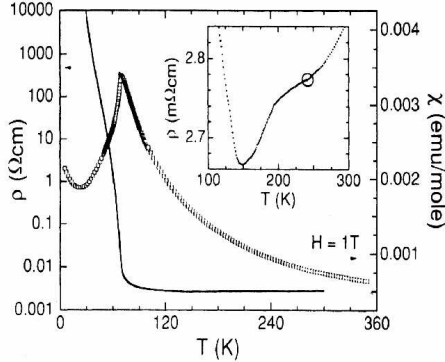


Fig. 5. Electrical resistivity (full line) and magnetic susceptibility (circles) of BaVS₃ (from Ref. 22)).

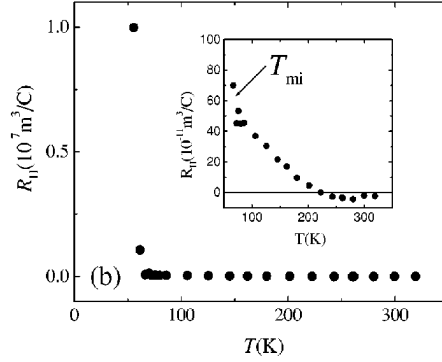


Fig. 6. Hall coefficient R_H versus temperature. The large increase close to T_{MIT} indicates the carrier loss (from Ref. 23)).

is found to be $2k_F^{LDA} \simeq 0.94c^*$,³⁷⁾ while the observed wave vector of the instability is $q_{MIT} = 0.5c^*$.²⁸⁾ Therefore, the simple picture of a CDW at $q_{MIT} = 2k_F$ associated only with the A_{1g} band is untenable within LDA. It is likely that the E_g states also participate in the instability, still the LDA band structure does not provide a Fermi-surface nesting that is in line with experimental findings. Hence, ab-initio calculations based on L(S)DA are not sufficient to explain the complex electronic structure of BaVS₃. Static L(S)DA+U and/or GGA+U schemes appear also not to be adequate. Despite the fact that a band gap is obtained for $Cmc2_1$ -BaVS₃ when enforcing magnetic order, this does not resemble the experimental scenario of an CDW mechanism underlying the transition from a Curie-Weiss-like metal into an paramagnetic insulator.

In the following we will show that within a DMFT framework, using the LDA electronic structure as a starting point, one may indeed reconcile theory with experimental findings. On the basis of this LDA+DMFT treatment we propose correlation effects in a multi-orbital context as an explanation for the discrepancies between band theory predictions and experiments, in line with the results of our model investigations in §2. Specifically, we show that interorbital charge transfers occur which lower the occupancy of the A_{1g} orbital in favor of the E_g 's. Thus leading to a Fermi surface modification by mainly shifting $k_F(A_{1g})$ towards lower values. From a calculation of the local susceptibilities, we demonstrate that local moments are formed in the metallic phase due to the low quasiparticle coherence scale induced by the strong correlations (in particular for the narrow E_g bands).

3.2. Computational Approach

We performed a realistic many-body investigation of the electronic structure of BaVS₃ by means of the combination of the LDA with the DMFT. The ab-initio LDA calculations were performed with a pseudopotential code within a mixed-basis consisting of plane waves and localized functions.³⁸⁾ Norm-conserving pseudopotentials were used, and for the exchange-correlation functional the parametrization of

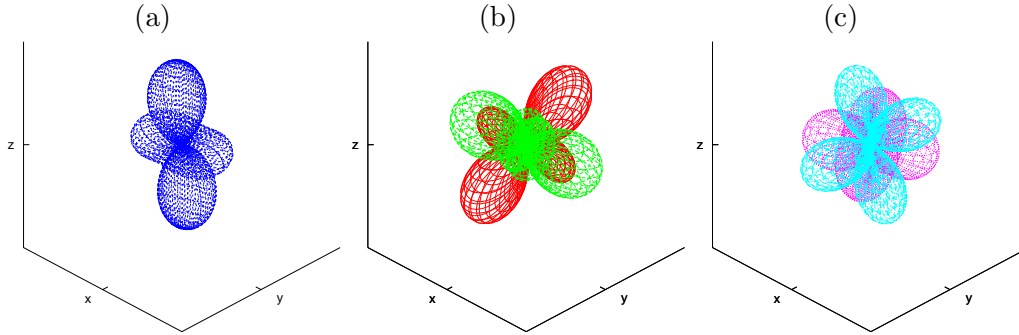


Fig. 7. Symmetry adapted $V(3d)$ orbitals for BaVS_3 in the $Cmc2_1$ structure. (a) A_{1g} , (b) E_g as well as (c) e_g . In the orthorhombic $Cmc2_1$ structure the following correspondence for the axes is realized: $a \leftrightarrow x$, $b \leftrightarrow y$, $c \leftrightarrow z$.

Perdew and Wang³⁹⁾ was utilized. In order to account for the given crystal symmetry of BaVS_3 , a symmetry-adapted $V(3d)$ -basis $\{\phi_m\}$ (see Fig.7) was obtained by diagonalizing the orbital density matrix $n_{MM'} \sim \sum_{\mathbf{k}b} f_{\mathbf{k}b} \langle \psi_{\mathbf{k}b} | M \rangle \langle M' | \psi_{\mathbf{k}b} \rangle$, where $\psi_{\mathbf{k}b}$ stands for the pseudo crystal wave function for wave vector \mathbf{k} and band b , and M, M' denote the cubic harmonics for $\ell=2$.

In the LDA+DMFT approach the on-site Green's function of a multi-orbital problem reads as

$$\mathbf{G}_\sigma(i\omega_n) = \sum_{\mathbf{k}} [(i\omega_n + \mu)\mathbf{1} - \mathbf{H}(\mathbf{k}) - \mathbf{\Sigma}_\sigma(i\omega_n)]^{-1} \quad , \quad (3.1)$$

with $\mathbf{H}(\mathbf{k})$ as the self-consistent determined LDA hamiltonian, provided in a localized basis, as well as the k -independent self-energy $\mathbf{\Sigma}(i\omega_n)$. In Eq. (3.1), σ is the spin index, $\omega_n = (2n+1)\pi/\beta$ ($n = 0, \pm 1, \pm 2, \dots$) are the fermionic Matsubara frequencies for the inverse temperature $\beta \equiv T^{-1}$, and μ is the chemical potential. For the special matter in hand, we restricted the calculations to the paramagnetic case, because no magnetic order is expected in the MIT regime. Furthermore, we approximated the full LDA hamiltonian by its downfolded version onto the $\{A_{1g}, E_g\}$ basis, which is sufficient to capture the essential physics close to the MIT. This downfolding to an effective 3-band model was performed 'empirically', lead by straightforward physical arguments, on the LDA DOS.⁹⁾ The $V(3d)$ -Green's function matrix for the effective 3-band model takes diagonal shape in the LDA limit. We kept this shape also within the DMFT framework, since off-diagonal self-energy terms should be small due to symmetry. Thus one may replace the k -sum in eq. (3.1) by the integral over the partial DOS $D_m(\varepsilon)$, so that the orbital-resolved Green's functions are written as

$$G_m(i\omega_n) = \int \frac{d\varepsilon D_m^{(\text{LDA})}(\varepsilon)}{i\omega_n + \mu - \varepsilon - \Sigma_m(i\omega_n)} \quad , \quad m = A_{1g}, E_{g1}, E_{g2} \quad . \quad (3.2)$$

Note that by treating only correlated states in this realistic DMFT formalism, double-counting terms originating from correlations already included in the LDA are absorbed by the chemical potential μ . The on-site vertex was again parametrized as

$U_{mm}^{\uparrow\downarrow}=U$, $U_{m\neq m'}^{\uparrow\downarrow}=U-2J$ and $U_{m\neq m'}^{\uparrow\uparrow(\downarrow\downarrow)}=U-3J$, with U the on-site Coulomb repulsion and J the local Hund's rule coupling. Recall that J does not only describe the spin exchange energy, but also the reduction of U for electrons in different orbitals. The local impurity problem within the DMFT formalism was again solved using QMC with similar convergence parameters as in the model investigations.

3.3. The electronic structure within LDA

Figure 8 shows the computed band structure for the $Cmc2_1$ crystal data at $T=100$ K.²⁶⁾ The high-symmetry points Γ - C - Y define a triangle in the $k_z=0$ plane, whereas Z - E - T is the analog shifted triangle in the $k_z=0.5c^*$ plane. The Γ - Z line corresponds to the propagation along the chain direction in $BaVS_3$. Also drawn are the so-called fatbands for the $\{A_{1g}, E_g\}$ orbitals. The width of these fatbands is proportional to the amount of the orbital character of a given band in the symmetry-adapted $\{\phi_m\}$ basis. Being directed along the chain direction between pairs of V atoms, the A_{1g} orbital has mainly d_{z^2} character. In contrast, the E_g states, linear combinations of d_{yz} , $d_{x^2-y^2}$ and d_{z^2} (E_{g1}) as well as d_{xy} and d_{xz} (E_{g2}), only weakly hybridize with their surrounding. The orbitals of the remaining e_g manifold point mainly towards the sulfur atoms, which results in a large energy splitting, leading to a smaller(larger) contribution to the occupied(unoccupied) states well below(above) ε_F . Therefore, the e_g states do not have a major influence on the essential physics around the MIT. In Fig. 8 one can clearly identify that the very narrow bands at the Fermi level are associated with the two E_g orbitals. Along Γ - Z starting at around -1 eV, one observes a nearly filled dispersive band with mainly A_{1g} character that crosses the Fermi level close to the edge of the Brillouin zone (BZ). The $2k_F$ value for this band amounts to $0.94c^*$, hence is incompatible with the experimentally observed $2k_F=0.5c^*$ instability. In addition, the filling of the E_g bands is rather low and cannot account for the observed magnitude of the local moment. Note however

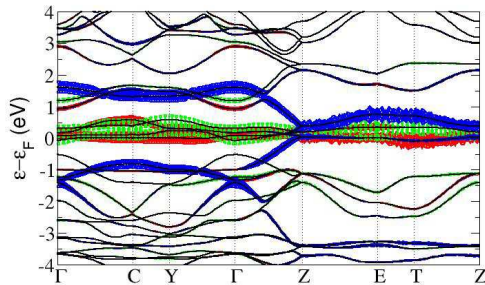


Fig. 8. LDA band structure for $Cmc2_1$ - $BaVS_3$ along high-symmetry lines in the 1. Brillouin Zone. Also shown are the fatbands (see text) for the A_{1g} (blue), E_{g1} (red) and E_{g2} (dashed-green) orbital of the V atoms. The wiggling of the fatbands in the Z - E - T plane is due to the high degeneracy of the bands.

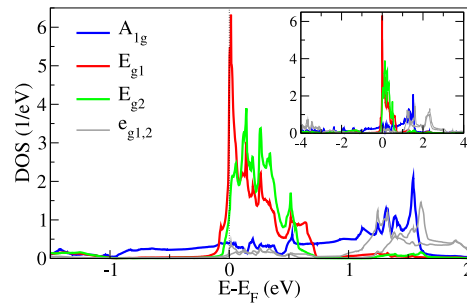


Fig. 9. Partial LDA-DOS of the V(3d) states in the symmetry-adapted basis. For the computation of this partial DOS, a sphere of radius 2.18 a.u., i.e., half of the nearest-neighbor V-S distance, was introduced.

the small E_{g2} electron pocket at the Γ point. It is absent in the band structure of the hexagonal phase and may be related to the hole-like conduction below T_S as seen in Hall measurements.²³⁾ The relevant k -summed electronic structure can be examined in Fig. 9 via the ϕ_m -resolved LDA-DOS per atom of the V($3d$) states. This plot of the partial DOS is characterized around the energy intervall $[-1,2]$ eV by a rather broad A_{1g} band and two strikingly narrow E_g bands right at E_F , in accordance with the shown band structure. The small crystal-field splittings read: $\Delta(A_{1g}, E_g) = \varepsilon_{A_{1g}} - \varepsilon_{E_g} \sim 0.1$ eV and $\Delta(E_{g1}, E_{g2}) = \varepsilon_{E_{g1}} - \varepsilon_{E_{g2}} \sim -0.05$ eV.

3.4. Orbital repopulations and Fermi surface deformations

We will show that the intimate interplay between the Hubbard parameters U and J as well as the given LDA band dispersions can eventually result in a substantial charge transfer from the broader A_{1g} band to the narrower E_g bands. Additionally, accompanied by this charge transfer is a shift of the A_{1g} band in k -space, providing the possibility for the onset of the experimentally detected CDW instability.

Due to the lack of information about the value of U in BaVS₃ from experiment (e.g., photoemission) or theory (constrained LDA methods tend to underestimate the screening for metals), we undertook our investigation by carefully scanning through the physically meaningful U - J parameter space for this compound. Since the interplay of U and J appears to be a central issue, we chose to fix the ratio U/J . By varying U we studied two different series: $U/J=7$ and $U/J=4$. Recall that in the 2-band model we encountered in §2, the ratio $U/J=5$ separated the polarization/compensation regimes in the static limit. One would expect to find similar regimes also in the present 3-band model for BaVS₃.

The orbital occupancies in our effective 3-band model, at the LDA level (i.e., for $U=0$) read: $n(A_{1g})=0.712$, $n(E_{g1})=0.207$ and $n(E_{g2})=0.081$. In Fig. 10a we plotted the respective band fillings in the metallic regime for increasing U within the two U/J series. The main effect apparent on Fig. 10a is that moderate correlations indeed tend to bring the occupancies of each orbital closer to one another, i.e., to decrease the population of the “extended” A_{1g} orbital and to increase the occupancy of the E_g orbitals. For strong correlations, values close to $n(A_{1g}) \simeq n(E_{g1}) + n(E_{g2}) \simeq 0.5$ are obtained in the DMFT calculation, corresponding to a half-filled band. The difference in the qualitative U -dependence of the band fillings between the two U/J series resembles those of the model calculations. For $U/J=4$ there is an immediate orbital charge transfer for $U \neq 0$, whereas for $U/J=7$ correlations first have to overcome the polarizing tendencies for small U . Hence the basic mechanisms found in the model calculations appear to be an essential point in understanding the physics of BaVS₃. Note that observations on the importance of J and of band-narrowing effects for the band filling in realistic systems have also been pointed out in the context of ruthenates.^{2),8)} For $U \sim 4$ eV the system reaches the Mott transition within $U/J=7$, whereas this transition is shifted to much larger U values for $U/J=4$. In the present context, we did not investigate the Mott insulating state as this one may not be relevant for realistic BaVS₃. Recall that in nature the orthorhombic ($Cmc2_1$) structure transforms at T_{MIT} via an CDW instability into a monoclinic (Cm) structure with 4 inequivalent vanadium atoms in the unit cell. Hence an understanding of the true

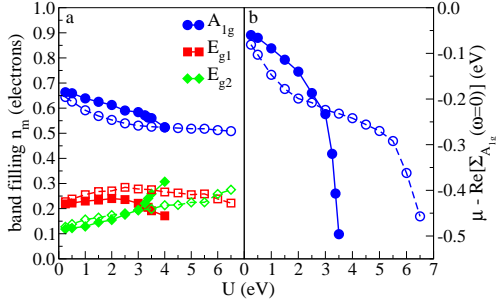


Fig. 10. (a) Band fillings at $\beta=(k_B T)^{-1}=15$ eV^{-1} ($T=774$ K) for the effective bands within LDA+DMFT. (b) Corresponding shift of the Fermi level for the A_{1g} band (note that $\varepsilon_{\mathbf{k}_F}^{\text{LDA}}=0$). Filled symbols: $U/J=7$, open symbols: $U/J=4$.

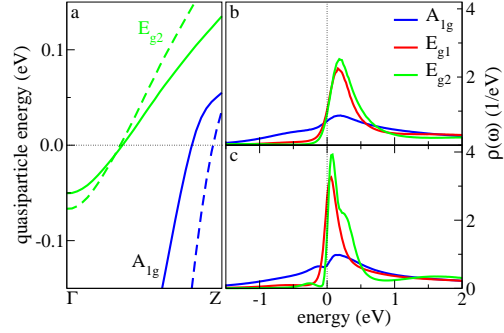


Fig. 11. LDA+DMFT spectral data for $U=3.5$ eV, $U/J=4$. (a) $V(3d)$ low-energy quasiparticle bands along Γ -Z in LDA (dashed lines) and LDA+DMFT (solid lines) for $T=332$ K. (b,c) integrated spectral function $\rho(\omega)$ for a single formula unit of BaVS_3 at $T=1160$ K (b) and $T=332$ K (c).

insulating state cannot be obtained by driving the system in the Mott-insulating regime. For the strongly correlated metal close to T_{MIT} we would estimate $U \sim 3.5$ eV in order to explain the substantial filling of the E_g states revealed from the local moment examinations.

As already noted, the correlation-induced orbital charge transfers not only modify the respective band fillings, but may lead also to relevant changes of the Fermi surface. Such an effect is anticipated in the case of BaVS_3 due to the insufficiency of DFT in LDA to explain the observed CDW instability. Indeed our calculations reveal that the depletion of the A_{1g} band is accompanied by a reduction of the corresponding Fermi wave vector \mathbf{k}_F along the Γ -Z direction. While a full determination of the quasiparticle (QP) band structure in the interacting system requires a determination of the real-frequency self-energy, we can extract the low-energy expansion of this quantity from our QMC calculation in the form: $\text{Re}\Sigma_m(\omega+i0^+) \simeq \text{Re}\Sigma_m(0) + \omega(1-1/Z_m) + \dots$, with Z_m the QP residue associated with each orbital. The poles of the Green's function determine the QP dispersion relation: $\det[\omega_{\mathbf{k}} - \hat{Z}[\hat{H}_{\mathbf{k}}^{\text{LDA}} + \text{Re}\hat{\Sigma}(0) - \mu]] = 0$, with μ the chemical potential. Focusing first on the A_{1g} sheet of the Fermi surface, within our diagonal formulation the location of the Fermi wave vector in the interacting system is determined by: $\varepsilon_{A_{1g}}^{\text{LDA}}(\mathbf{k}_F) = \mu - \text{Re}\Sigma_{A_{1g}}(0)$. This quantity therefore yields the energy shift of the A_{1g} band at the Fermi surface crossing, as compared to LDA. It is depicted in Fig. 10b as a function of U . In Fig. 11a, we display the QP bands that cross the Fermi level along Γ -Z in a narrow energy range around ε_F for $U=3.5$ eV in the $U/J=4$ series. The QP bands are obtained by performing a perturbative expansion of the pole equation above, which yields: $\omega_{b\mathbf{k}} = \sum_m C_{m\mathbf{k}}^b Z_m [\varepsilon_{b\mathbf{k}}^{\text{LDA}} + \text{Re}\Sigma_m(0) - \mu]$ with $C_{m\mathbf{k}}^b \equiv |\langle \psi_{b\mathbf{k}} | \phi_m \rangle|^2$ the LDA orbital weight. From these two figures, it is clear that $k_F(A_{1g})$ is reduced in comparison to the LDA value, in line with the global charge transfer from A_{1g} to E_g . This opens new possibilities for the CDW instability, in particular for the nesting wave vector.

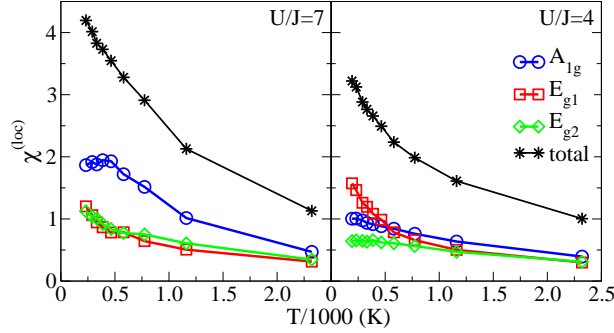


Fig. 12. Temperature-dependent local spin susceptibilities for $U=3.5$ eV, according to the normalization $\chi^{(\text{loc})} = \int_0^\beta d\tau \langle \hat{S}_z(0) \hat{S}_z(\tau) \rangle$, where \hat{S}_z denotes the z -component of the spin operator.

The enhanced population of the narrow E_g bands, as well as the correlation-induced reduction of its bandwidth (see Fig. 11a) provide an explanation for the local moments observed in the metallic phase. To support this, we have calculated (Fig. 12) the local susceptibility associated with each orbital $\chi_m^{(\text{loc})} \equiv \sum_{\mathbf{q}} \text{Re}[\chi_m(\mathbf{q}, \omega=0)]$. For both values of U/J , the susceptibility of the A_{1g} band saturates to a Pauli-like value at low temperatures. In contrast, $\chi^{(\text{loc})}$ of the E_g orbitals strongly increases as the temperature is lowered (except for the low-filled E_{g2} orbital at $U/J=4$). This is because the coherence temperature below which quasiparticles form is much lower for the E_g orbitals than for the A_{1g} orbital. Accordingly, our calculation of the integrated spectral functions (Fig. 11b,c) reveals a strong T -dependence of the E_g QP peak. Some differences between the two series are clear from Fig. 12. For $U/J=7$, the system is already very close to the Mott transition when choosing $U=3.5$ eV. Thus the A_{1g} electrons also act as local moments over part of the temperature range, while for $U/J=4$ and same U , the T -dependence of the total local susceptibility is almost entirely due to the E_{g1} electrons. Which of the two situations is closest to the physics of BaVS₃ does require further investigations, albeit some experimental indications point at the second possibility.⁴⁰⁾

§4. The Fermi surface of Na_{*x*}CoO₂

Since the surprising discovery of superconductivity in Na_{*x*}CoO₂·*y*H₂O⁴¹⁾ for $x \sim 0.35$, the sodium cobaltate system has made its way to one of the hottest topics in current research on strongly correlated materials. The layered CoO₂ oxides, held together by Na layers in between, resemble the famous cuprates, although the Co atoms form a triangular lattice with the oxygen atoms in a pyramidal configuration above and below the Co plane. Besides the superconducting phase the unhydrated sodium cobaltates exhibit additional rich physics, such as strong electric thermopower,⁴²⁾ charge order,⁴³⁾ different magnetic order,⁴⁶⁾ as well as complex ordering of the Na atoms.⁴⁴⁾ Bounded by a Mott-Hubbard insulator for $x=0$, i.e., CoO₂, and by the band insulator NaCoO₂ for $x=1$, the sodium cobaltate phase diagram⁴⁵⁾ is roughly separated in a Pauli-like metallic region for $x < 0.5$ and a Curie-Weiss-like metallic

region for $x > 0.5$. In another difference to the cuprates, cobaltate is a multi-orbital $3d^{5+x}$ system. Due to the crystal-field splitting the Co atoms are in a low-spin state, hence the d electrons occupy the lower t_{2g} band complex (i.e., there are $1 - x$ holes in the t_{2g} shell). It follows that the Curie-Weiss behavior stems from Co^{4+} local moments, whereas these moments seem to disappear below $x = 0.5$. Interestingly, magnetic phases are experimentally verified for $x \geq 0.75$.⁴⁶⁾

From this short introduction of Na_xCoO_2 it is already obvious that the $x = 0.5$ composition plays a subtle role in this system. Although the characteristics of the phase at $x = 0.5$ are still not completely resolved, certain properties seem to be established. In contrast to most other doping levels x , $\text{Na}_{0.5}\text{CoO}_2$ exhibits an ordered superstructure for the combined Na/CoO_2 system⁴⁷⁾ over a wide temperature range. Most importantly, $\text{Na}_{0.5}\text{CoO}_2$ shows a MIT at ~ 53 K. If this transition is truly associated with the onset of charge ordering is still a matter of debate, although many measurements point in this direction.^{45), 48)} There appear to be⁴⁷⁾ additional magnetic and/or structural transitions at 20 K and 87 K.

Early electronic structure calculations in the L(S)DA framework for $\text{Na}_{0.5}\text{CoO}_2$ have been performed by Singh.⁴⁹⁾ Since the the ordered superstructure was identified only recently, in these DFT calculations a disordered arrangement of the sodium atoms was assumed (treated within the virtual crystal approximation). The Fermi surface revealed in this investigation exhibits a large cylindrical hole sheet with dominant A_{1g} character around the Γ - A line in the Brillouin zone of the hexagonal unit cell, as well as small hole pockets in the Γ - K and A - H directions. This topology of the Fermi surface appears to be rather generic for a wide range of x within the LDA framework. It has been suggested⁵⁰⁾ that strong nesting between the hole pockets leads to large fluctuations in the spin channel, having important influence on the character of the superconducting state at $x \sim 0.35$. However the existence of these hole pockets has not been confirmed in angle-resolved photoemission (ARPES) experiments.^{51), 16), 17)} On the contrary, in one of these ARPES measurements¹⁶⁾ the ‘‘pocket’’ bands were found well below the Fermi level for large doping range x .

It appears obvious from the latter discussion that Fermi-surface modifications due to strong correlation effects may play also an important role for sodium cobaltates. Hence the last sections are devoted to a brief analysis of the problem of finding the correct generic Fermi surface for Na_xCoO_2 .

4.1. Electronic structure within LDA

In order to have a well-defined starting point, we tried to find theoretical agreement with the experimentally detected ordered superstructure for $\text{Na}_{0.5}\text{CoO}_2$. Thus we performed total energy calculations with the mixed-basis pseudopotential (MBPP) code for different arrangements of sodium atoms in the interlayers in between the CoO_2 planes. As a starting point for the Na_xCoO_2 structural model one usually utilizes the hexagonal ($P6_322$ or $P6_3/mmc$) symmetry.^{52), 49), 47)} In all our studies the lattice parameters were confined to the values obtained by Jansen and Hoppe,⁵²⁾ i.e., $a_H = 2.84 \text{ \AA}$ and $c_H = 10.81 \text{ \AA}$. Indeed we obtained the lowest LDA total energy for the experimentally suggested superstructure with global orthorhombic ($Pmnm$) symmetry.⁴⁷⁾ We relaxed the atomic positions within the MBPP and the corre-

sponding superlattice is depicted in Fig. 13. The unit cell of this superstructure with dimension $a_O=2a_H, b_O=a_H\sqrt{3}$ and $c_O=c_H$ contains 28 atoms, whereby there are 2 inequivalent Na and Co sites, respectively, as well as 3 inequivalent O sites. The two classes of inequivalent Na and Co sites are related as the Na ordering is such that in each sodium interlayer there are atoms sitting on top of an Co site (Na1/Co1) and such atoms that are placed on top of an oxygen site (Na2) (see. Fig. 13b). The Co atoms without an Na atom on top form the Co2 class. As reported by Huang *et al.*,⁴⁷⁾ this ordered superstructure should be stable over a wide temperature range, with possible structural changes below 100 K.

We determined the LDA electronic structure for the $Pmmn$ symmetry with the MBPP code (a similar study was published recently⁵³⁾). The resulting band structure and the symmetry-adapted $3d$ -DOS for the two Co classes are shown in Fig. 14 and Fig. 15. The band structure around the Fermi level consists of 3 isolated blocks. Roughly speaking, the block deep in energy is formed by the O($2p$) states and the one high in energy stems from the Co(e_g) states. The most interesting block of bands close to the Fermi level is mainly dominated by the Co(t_{2g}) multiplet and has only minor O($2p$) weight due to the remaining Co(t_{2g})-O($2p$) hybridization. Thereby, the A_{1g} subband complex is characterized by an substantial bonding-antibonding splitting, in between which the E_g subband complex is mainly located. A crystal-field splitting of $\Delta=\varepsilon_{A_{1g}} - \varepsilon_{E_g} \sim -0.1$ eV between these two band complexes can be derived. The crystal-field splitting between the different E_g states appears to be negligible. From Fig. 15 no striking difference between the electronic states within the named t_{2g} multiplet for the two Co classes, i.e., Co1 and Co2, can be extracted. For the respective LDA orbital occupations the following inequalities hold: $n_{t_{2g}}^{(Co1)} > n_{t_{2g}}^{(Co2)}$ and $n_{E_{g1}, E_{g2}} > n_{A_{1g}}$. Hence the two Co classes are discriminated

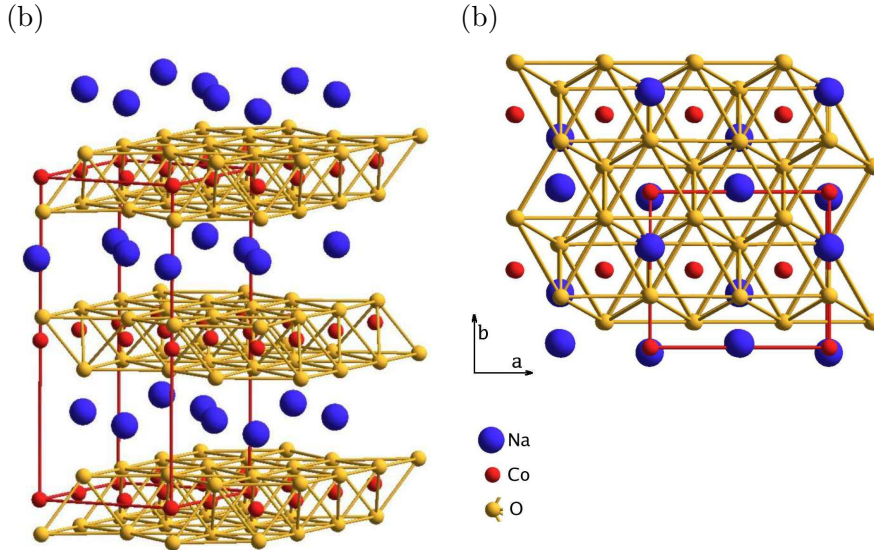


Fig. 13. $\text{Na}_{0.5}\text{CoO}_2$ in the orthorhombic ($Pmmn$) structure. (a) 3D view, (b) view along the c axis.

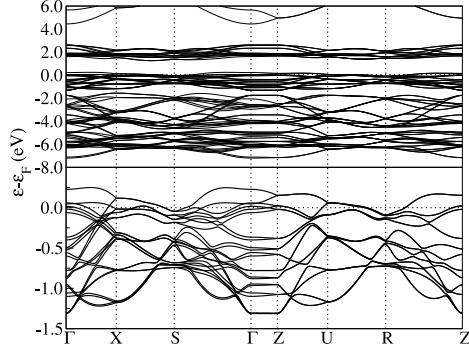


Fig. 14. LDA band structure for $\text{Na}_{0.5}\text{CoO}_2$ in the $Pmmn$ crystal structure along high-symmetry lines in the 1. BZ of the orthorhombic lattice.

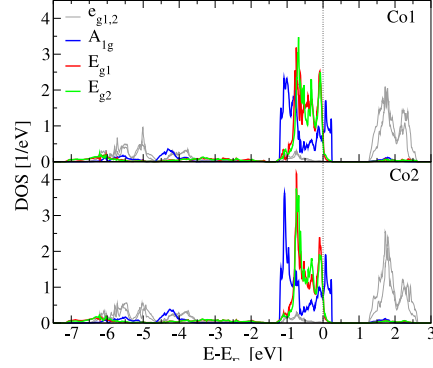


Fig. 15. Partial LDA-DOS of the $\text{Co}(3d)$ states in the symmetry-adapted basis for Co1 and Co2 atoms.

in LDA by a minor charge disproportionation (~ 0.06 electrons), and the results support the suggestion⁴⁷⁾ that the Co1 atoms should tend to the lower oxidation state, i.e., Co^{3+} rather than Co^{4+} . However in this work we do not address the question of charge ordering. Finally, the hole occupancy is enlarged in the A_{1g} orbital for both Co classes.

For the discussion of the LDA Fermi surface we plotted in Fig. 16 also the band structure close to the Fermi level for the larger ($a=a_H$) hexagonal BZ (with symmetry lines in direct comparison to Singh's work⁴⁹⁾), since the generic Na_xCoO_2 system is most often associated with the hexagonal symmetry stemming from the CoO_2 sublattice. In this representation higher BZs of the orthorhombic structure are touched, thus the band structure exhibits some folding. We also provide the fatbands for the respective t_{2g} orbitals in Fig. 17. By comparing the band structure of the ordered superstructure in Fig. 16 with the one assuming disordered sodium interlayers in a

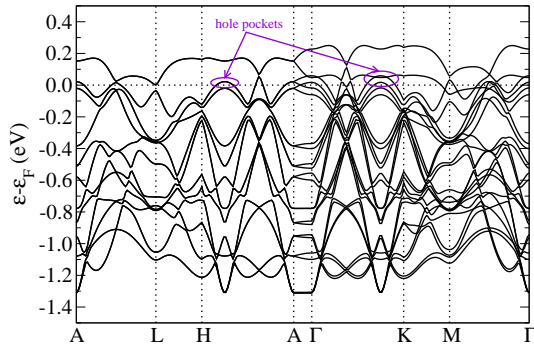


Fig. 16. LDA band structure for $\text{Na}_{0.5}\text{CoO}_2$ in the $Pmmn$ crystal structure along high-symmetry lines in the 1. BZ of the hexagonal lattice with $a=a_H$.

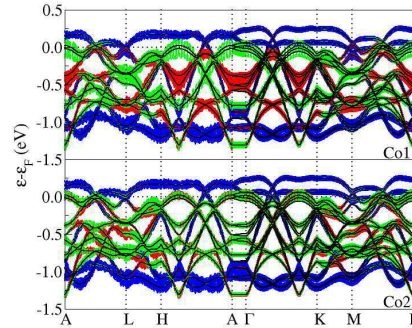


Fig. 17. t_{2g} fatbands for the Co1 and Co2 class in the hexagonal BZ (A_{1g} :blue, E_{g1} :red and E_{g2} :green).

smaller unit cell from Ref. 49), some differences may be identified. There are bands in the $A-\Gamma$ direction right at the Fermi level which result in an additional Fermi surface sheet for the orthorhombic structure. ARPES intensity close to the Γ point has been detected recently but below the Fermi level.¹⁶⁾ In the same ARPES study the famous pocket bands were found *below* the Fermi level, whereas in our LDA calculation they form, of course, still hole Fermi sheets. It is instructive to study the main orbital character of the relevant bands within the t_{2g} block. From Fig. 17, the hole pockets are nearly exclusively stemming from the E_g orbitals of Co. The same holds for the bands along $A-\Gamma$ at the Fermi level. As a general subtle difference between Co1 and Co2, one observes that in the case of Co1 the E_g bands have either E_{g1} or E_{g2} character, whereas for Co2 these bands have mixed $E_{g1,2}$ character. Since the large hole Fermi sheet has dominant A_{1g} character ARPES measurements suggest a strong orbital polarization for $\text{Na}_{0.5}\text{CoO}_2$, namely with nearly entirely filled E_g bands and A_{1g} hole bands with a filling close to 0.5 holes per Co atom.

4.2. Pockets or no pockets?

Since the t_{2g} -manifold bandwidth W is very narrow, Na_xCoO_2 is expected to be in the regime of strong correlations $W \ll U$. This is qualitatively consistent with the substantial mass renormalization and high thermopower. A value of $U \approx 4$ eV has been estimated.⁵⁴⁾ Hence, considerations from DFT-LDA may not provide the correct picture of the electronic structure, even for the Fermi surface itself. In a recent LDA+U calculation¹⁸⁾ the pocket bands were shifted below the Fermi energy for various dopings x (corresponding to increased orbital polarization), in agreement with the ARPES measurements. We have also performed (unpublished) LDA+U calculations of orthorhombic $\text{Na}_{0.5}\text{CoO}_2$ and confirm this result. However, the static LDA+U approach is certainly questionable for the metallic regime of $\text{Na}_{0.5}\text{CoO}_2$. Moreover, the precise shape of the Fermi surface in LDA+U depends on the specific choice of the double-counting correction terms. Recently, an LDA+DMFT calculation¹⁰⁾ obtained the opposite effect for realistic values of J , namely a further stabilization of the hole pockets compared to LDA. In contrast, another study based on the Gutzwiller approximation reported that the hole pockets were shifted below the Fermi level,¹¹⁾ but this is perhaps not surprising since $U \rightarrow \infty$ and $J=0$ were used in this calculation, hence favoring orbital polarization. Note that the sodium cobaltates have non-integer total hole filling $(1-x) \in [0,1]$ per Co atom. As explored in §2, the direction of the charge flow leading to orbital compensation or polarization is the result of a delicate balance between different parameters, namely: the total filling, the Hund's rule coupling, the crystal-field splitting, and the bandwidth of each band (taking into account the renormalization of the latter two by strong correlations). Further studies are therefore necessary to fully settle the issue for Na_xCoO_2 . To conclude, let us emphasize that the following aspects, neglected in previous studies, might be important in order to reach this goal:

- Non-diagonal terms $\Sigma_{mm'}$ in the self-energy, renormalizing the interorbital hybridizations and therefore influencing charge flows.
- Spin-flip and pair-hopping (non-Ising) terms in the Coulomb vertex.
- Importantly, an *orbital-independent* double-counting correction within the t_{2g}

multiplet has usually been assumed when including dynamical correlations. While orbital-dependence of this correction is expected to be rather small and hence should not affect significantly our conclusions for the larger charge-transfer effects in the case of BaVS₃, it may play a substantial role in the more delicate case of Na_xCoO₂.

- Finally, non-local effects might be important, such as those induced by a strong interatomic Coulomb interaction. The latter have been proposed⁵⁵⁾ to be important for the cobaltates, as also suggested by the observed tendency to charge ordering.

Acknowledgements

We would like to acknowledge useful discussions with J.W. Allen, H. Alloul, S. Fagot, P. Fazekas, L. Forró, P. Foury-Leylekian, J. Geck, M.D. Johannes, P.A. Lee, A. Liebsch, A. Millis, J.-P. Pouget and S. Ravy. This work was supported by École Polytechnique and CNRS, as well as by the “Psi-k *f*-electron” Network (HPRN-CT-2002-00295) and a grant of supercomputing time at IDRIS Orsay (project 051393).

References

- 1) V.I. Anisimov, A.I. Poteryaev, M.A. Korotin, A.O. Anokhin, and G. Kotliar, J. Phys. Cond. Matter **9** (1997), 7359; A.I. Lichtenstein and M.I. Katsnelson, Phys. Rev. B **57** (1998), 6884.
- 2) A. Liebsch and A. Lichtenstein, Phys. Rev. Lett. **84** (2000), 1591.
- 3) E.K.R. Runge, R.C. Albers, N.E. Christensen, and G.E. Zwicknagl, Phys. Rev. B **51** (1995), 10375.
- 4) C.S. Wang and J. Callaway, Phys. Rev. B **9** (1973), 4897; F. Weling and J. Callaway, Phys. Rev. B **26** (1982), 710.
- 5) I. Yang, S.Y. Savrasov, and G. Kotliar, Phys. Rev. Lett. **87** (2001), 216405.
- 6) J.M. Luttinger, Phys. Rev. **119** (1960), 1153.
- 7) E. Pavarini, S. Biermann, A. Poteryaev, A.I. Lichtenstein, A. Georges, and O.K. Andersen Phys. Rev. Lett. **92** (2004), 176403
- 8) S. Okamoto and A.J. Millis, Phys. Rev. B **70** (2004), 195120.
- 9) F. Lechermann, S. Biermann, and A. Georges, Phys. Rev. Lett. **94** (2005), 166402.
- 10) H. Ishida, M.D. Johannes, and A. Liebsch, cond-mat/0412654.
- 11) S. Zhou, M. Gao, H. Ding, P.A. Lee, and Z. Wang, cond-mat/0503346.
- 12) C. Castellani, C. R. Natoli, and J. Ranninger, Phys. Rev. B **18** (1978), 4945; R. Frésard and G. Kotliar, Phys. Rev. B **56** (1997), 12909.
- 13) N. Manini, G.E. Santoro, A. Dal Corso, and E. Tosatti, Phys. Rev. B **66** (2002), 115107.
- 14) For a review see A. Georges, G. Kotliar, W. Krauth and M.J. Rozenberg, Rev. Mod. Phys. **68**, 13 (1996).
- 15) J.E. Hirsch and R.M. Fye, Phys. Rev. Lett. **56**, 2521 (1986).
- 16) H.-B. Yang, Z.-H. Pan, A.K.P. Sekharan, T. Sato, S. Souma, T. Takahashi, R. Jin, B.C. Sales, D. Mandrus, A.V. Fedorov, Z. Wang, and H. Ding, cond-mat/0501403.
- 17) J. Geck, B. Büchner, T. Kroll, H. Berger, S. Borisenko, D. Chen, S.-L. Drechsler, J. Fink, C. Hess, M. Knupfer, A. Kordyuk, G. Krabbes, C. Lin, H. Rosner, C. Sekar, and V. Zabolotnyy, 2005 (unpublished).
- 18) P. Zhang, W. Luo, M.L. Cohen, and S.G. Louie, Phys. Rev. Lett. **93** (2004), 236402.
- 19) M. Takano, H. Kosugi, N. Nakanishi, M. Shimada, T. Wada, and M. Koizumi, J. Phys. Soc. Jpn. **43** (1977), 1101.
- 20) O. Massenet, J.J. Since, J. Mercier, M. Avignon, R. Buder, and V.D. Nguyen, J. Phys. Chem. Solids **40** (1979), 1.
- 21) K. Matsuhara, T. Wada, T. Nakamizo, H. Yamauchi, S. Tanaka, Phys. Rev. B **43** (1991),

- 13118.
- 22) T. Graf, D. Mandrus, J.M. Lawrence, J.D. Thompson, P.C. Canfield, S.-W. Cheong, and L.W. Rupp Jr., Phys. Rev. B **51** (1995), 2037.
 - 23) C.H. Booth, E. Figueroa, J. M. Lawrence, M.F. Hundley, and J.D. Thompson, Phys. Rev. B **60** (1999), 14852.
 - 24) M.H. Whangbo, H.J. Koo, D. Dai, and A. Villesuzanne, J. Solid State Chem. **165**, 345 (2002).
 - 25) R. Gardner, M. Vlasse, and A. Wold, Acta Crystallogr. Sec. B **25** (1969), 781.
 - 26) M. Ghedira, M. Anne, J. Chenevas, M. Marezio, and F. Sayetat, J. Phys. C **19** (1986), 6489.
 - 27) H. Nakamura, T. Yamasaki, S. Giri, H. Imai, M. Shiga, K. Kojima, M. Nishi, K. Kakurai, and N. Metoki, J. Phys. Soc. Jpn. **69** (2000), 2763.
 - 28) S. Fagot, P. Foury-Leylekian, S. Ravy, J.-P. Pouget, and H. Berger, Phys. Rev. Lett. **90** (2003), 196401.
 - 29) T. Inami, K. Ohwada, H. Kimura, M. Watanabe, Y. Noda, H. Nakamura, T. Yamasaki, M. Shiga, N. Ikeda, and Y. Murakami, Phys. Rev. B **66** (2002), 073108.
 - 30) S. Fagot, P. Foury-Leylekian, S. Ravy, J.-P. Pouget, M. Anne, G. Popov, M. V. Lobanov, and M. Greenblatt, cond-mat/0410110.
 - 31) S. Huijzinga, J. Kommandeur, H.T. Jonkman, and C. Haas, Phys. Rev. B **25** (1982), 1717.
 - 32) G. Mihály, I. Kézsmárki, F. Záborszky, M. Miljak, K. Penc, P. Fazekas, H. Berger, and L. Forró, Phys. Rev. B **61** (2000), R7831.
 - 33) R. Itti, T. Wada, K. Matsuura, T. Itoh, K. Ikeda, H. Yamauchi, N. Koshizuka, and S. Tanaka, Phys. Rev. B **44** (1991), 2306.
 - 34) M. Nakamura, A. Sekiyama, H. Namatame, A. Fujimori, H. Yoshihara, T. Ohtani, A. Misu, and M. Takano, Phys. Rev. B **49** (1994), 16191.
 - 35) S. Mitrovic, P. Fazekas, C. Søndergaard, D. Ariosa, N. Barišić, H. Berger, D. Cloëtta, L. Forró, H. Höchst, I. Kupčić, D. Pavuna, G. Margaritondo, cond-mat/0502144.
 - 36) H. Imai, H. Wada, and M. Shiga, J. Phys. Soc. Jpn. **65** (1996), 3460.
 - 37) L.F. Mattheiss, Solid State Commun. **93** (1995), 791.
 - 38) B. Meyer, C. Elsässer, F. Lechermann and M. Fähnle, *FORTTRAN 90 Program for Mixed-Basis-Pseudopotential Calculations for Crystals*, Max-Planck-Institut für Metallforschung, Stuttgart, unpublished.
 - 39) J.P. Perdew and Y. Wang, Phys. Rev. B **45**, 13244 (1992).
 - 40) P. Fazekas, K. Penc, H. Berger, L. Forró, Sz. Csonka, I. Kézsmárki, and G. Mihály, Physica B **312-313** (1995), 694.
 - 41) K. Takada, H. Sakurai, E. Takayama-Muromachi, F. Izumi, R.A. Dilanian, and T. Sasaki, Nature **422** (2003), 53.
 - 42) I. Terasaki, Y. Sasago, and K. Uchinokura, Phys. Rev. B **56** (1997), R12685.
 - 43) I.R. Mukhamedshin, H. Alloul, G. Collin, and N. Blanchard, Phys. Rev. Lett. **93** (2004), 167601.
 - 44) H.W. Zandbergen, M. Foo, Q. Xu, V. Kumar, and R.J. Cava, Phys. Rev. B **70** (2004), 024101.
 - 45) M.L. Foo, Y. Wang, S. Watauchi, H.W. Zandbergen, T. He, R.J. Cava, and N.P. Ong, Phys. Rev. Lett. **92** (2004), 247001.
 - 46) J.L. Luo, N.L. Wang, G.T. Liu, D. Wu, X.N. Jing, F. Hu, and T. Xiang, Phys. Rev. Lett. **93** (2004), 187203.
 - 47) Q. Huang, M.L. Foo, J.W. Lynn, H.W. Zandbergen, G. Lawes, Y. Wang, B.H. Toby, A.P. Ramirez, N.P. Ong, and R.J. Cava, J. Phys.:Condens. Matter **16** (2004), 5803.
 - 48) N.L. Wang, D. Wu, G. Li, X.H. Chen, C.H. Wang, and X.G. Luo, Phys. Rev. Lett. **93** (2004), 147403.
 - 49) D.J. Singh, Phys. Rev. B **61** (2000), 13397.
 - 50) M.D. Johannes, I.I. Mazin, D.J. Singh, and D.A. Papaconstantopoulos, Phys. Rev. Lett. **93** (2004), 097005.
 - 51) M.Z. Hasan, Y.-D. Chuang, D. Qian, Y.W. Li, Y. Kong, A. Kuprin, A.V. Fedorov, R. Kimmeling, E. Rotenberg, K. Rossnagel, Z. Hussain, H. Koh, N.S. Rogado, M.L. Foo, and R.J. Cava, Phys. Rev. Lett. **92** (2004), 246402.
 - 52) M. Jansen and R. Hoppe, Z. Anorg. Allg. Chem. **408** (1974), 104.
 - 53) Z. Li, J. Yang, J.G. Hou, and Q. Zhu, Phys. Rev. B **71** (2005), 024502.

- 54) M.D. Johannes, I.I. Mazin, and D.J. Singh, cond-mat/0408696.
- 55) O.I. Motrunich and P.A. Lee, Phys. Rev. B **69** (2004), 214516; Phys. Rev. B **70** (2004), 024514.